ELSEVIER

Applied Mathematical Modelling 26 (2002) 89–111

APPLIED MATHEMATICAL MODELLING

www.elsevier.com/locate/apm

DEM modelling of industrial granular flows: 3D case studies and the effect of particle shape on hopper discharge

Paul W. Cleary *, Mark L. Sawley

Division of Mathematical and Information Sciences, CSIRO, Private Bag 10, Clayton South MDC, Vic., 3169, Australia

Received 1 December 1999; received in revised form 1 November 2000; accepted 24 April 2001

Abstract

While the discrete element method (DEM) is attracting increasing interest for the simulation of industrial granular flow, much of the previous DEM modelling has considered two-dimensional (2D) flows and used circular particles. The inclusion of particle shape into DEM models is very important and allows many flow features, particularly in hoppers, to be more accurately reproduced than was possible when using only circular particles. Elongated particles are shown here to produce flow rates up to 30% lower than for circular particles and give flow patterns that are quite different. The yielding of the particle microstructure resembles more the tearing of a continuum solid, with large-scale quasi-stable voids being formed and large groups of particles moving together. The flow becomes increasingly concentrated in a relatively narrow funnel above the hopper opening. This encourages the hope that DEM may be able to predict important problems such as bridging and rat-holing. Increasing the blockiness or angularity of the particles is also shown to increase resistance to flow and reduces the flow rates by up to 28%, but without having perceptible effect on the nature of the flow. We also describe our methodology for constructing and modelling geometrically complex industrial applications in three dimensions and present a series of industrially important three-dimensional (3D) case studies. The charge motion in a 5 m diameter ball mill and in a Hicom nutating mill, discharge from single- and four-port cylindrical hoppers, and particle size separation by a vibrating screen are demonstrated. For each case, plausible particle size distributions (PSDs) have been used. The results obtained indicate that DEM modelling is now sufficiently advanced that it can make useful contributions to process optimisation and equipment design. Finally the parallelisation of such a DEM code is described and benchmark performance results for a large-scale 2D hopper flow are presented.

* Corresponding author. Fax: +61-3-9545-8080.
E-mail address: paul.cleary@cmis.csiro.au (P.W. Cleary).

0307-904X/02/$ - see front matter
PII: S0307-904X(01)00050-6

1. Introduction

The flow of particulate materials plays a critical role in many industrial and mining processes. These range from crushing and grinding, blasting, separation (as in mineral liberation) and mixing (such as in glass making), to rotary moulding of plastics, commodity sampling (frequently from conveyor belts at discharge or interchange points), stockpile construction and discharge, open cut mining, excavation (including dragline operation) to generic particle flows in and from hoppers, silos, bins and conveyor belts. Small reductions in energy consumption or increases in output represent significant financial benefits for plant owners.

In the simulation of granular flows using the discrete element method (DEM) the trajectories, spins and orientations of all the particles are calculated, and their interaction with other particles and with their environment modelled. This method has been well established for simple flows for many years [1,2,24]. Two- and three-dimensional (3D) DEM simulations have been successfully applied to a range of industrial problems (see e.g. [5,6,16]). Particular application areas that have been studied using DEM simulation include dragline excavation [3], ball mill operation [4,14,15,19,23], silo filling [10] and mixing [11,17,26].

Despite the progress made to date, a number of further developments of DEM technology are required to enhance its applicability to real-world industrial problems. Two particular areas of importance involve improved physical modelling and the simulation of large-scale geometrically complex systems. Both of these aspects are examined in the present paper.

The flow of particulate material from hoppers has been a popular modelling problem for many years; see e.g. [13,18,20,21]. The relatively simple geometry and well-defined flow patterns have made it an attractive test case to study the capabilities of numerical simulation [10]. To date, the majority of DEM simulations have been two-dimensional (2D) and used mono-disperse or slightly poly-disperse distributions of discs. The flows predicted are generally far too fluid with the flow near the side walls being too rapid. Whilst DEM models can qualitatively predict mass flow, accurate predictions of funnel flow and phenomena such as rat-holing are yet to be obtained.

Two essential aspects that have been neglected in most DEM models are the effect of particle shape and inter-particle cohesion. Both contribute significantly to the shear strength of the granular assembly and determine where the material will fail and flow and when it will remain stationary. As a step towards developing realistic hopper flow models, a study of the effect of particle shape on the flow behaviour in a 2D hopper is presented. The change in flow pattern, discharge mass flow rate, discharge velocity and wall forces with the blockiness and aspect ratio of the particles are described.

Due to the presence of diverse scale lengths combined with geometrical complexity, typical minimum problem sizes for 3D industrial applications generally range from 20,000 to 100,000 particles with larger problems having millions of particles and the largest substantially more. 3D DEM simulations have to date been limited to the lower end of this range of complexity and size. Rapidly increasing computer speed and the development of parallel DEM codes allow larger-scale industrial problems to be explored.

In this paper we describe simulations of several geometrically-complex industrial applications. Issues of importance for large-scale 3D DEM simulations, including generating initial conditions, code parallelisation, and visualisation, are discussed.

2. The discrete element method

In discrete element simulation of granular flows the collisional interactions of particles with each other and with their environment are detected and modelled using a suitable contact force law. Equations of motion are then solved for the particle motions and for the motion of any boundary objects with which the particles interact. The general DEM methodology and its variants are well established and are described in review articles by Campbell [2], Barker [1] and Walton [24]. Here we use a reasonably standard implementation that is described in more detail in [3,5].

The particles are allowed to overlap and the amount of overlap Δx, and the normal v_n and tangential $\mathbf{v}_t$ relative velocities (at the contact point) determine the collisional forces via a contact force law. There are a range of possible contact force models available in the literature. These approximate the collision dynamics to various extents. We use a linear spring-dashpot model. For more complex models see [22,24].

The magnitude of the normal force is:

$$F_n = -k_n \Delta x + C_n v_n, \tag{1}$$

and consists of a spring to provide the repulsive force and a dashpot to dissipate a proportion of the relative kinetic energy. The maximum overlap between particles is determined by the stiffness k of the spring in the normal direction. Typically average overlaps of 0.1–1.0% are desirable, requiring spring constants of the order of 10^6–10^7 N/m in 2D and 10^4–10^6 N/m in 3D. The normal damping coefficient C_n is chosen to give a required coefficient of restitution ϵ (defined as the ratio of the post-collisional to pre-collisional normal component of the relative velocity):

$$C_n = 2\gamma\sqrt{m_{ij}k_n},$$

where

$$\gamma = -\frac{\ln(\epsilon)}{\sqrt{\pi^2 + \ln^2(\epsilon)}} \quad \text{and} \quad m_{ij} = \frac{m_i m_j}{m_i + m_j}$$

is the reduced mass of particles i and j with masses m_i and m_j respectively. This arises from the analytic solution of the normal collision equation (1) for two such particles.

The magnitude of the tangential force is given by:

$$\mathbf{F}_t = \min\left\{\mu F_n, k_t \int \mathbf{v}_t \, dt + C_t \mathbf{v}_t\right\}, \tag{2}$$

where the integral of the tangential velocity $\mathbf{v}_t$ over the collision behaves as an incremental spring that stores energy from the relative tangential motions and represents the elastic tangential deformation of the contacting surfaces. The dashpot dissipates energy from the tangential motion and models the tangential plastic deformation of the contact. The total tangential force (given by the sum of the elastic and plastic components) is limited by the Coulomb frictional limit at which point the surface contact shears and the particles begin to slide over each other.

In 2D the boundary objects are constructed from line segments, circular segments and discs. Nearly arbitrary shaped 2D mill cross sections can be built in this way. For 3D simulations, the

2D objects can be extruded into the third dimension or can be described by finite element meshes constructed from CAD using commercial mesh generators.

In this paper, the particles are modelled in 2D as either circular disks or as super-quadrics (for non-circular shapes) which are described by:

$$x^N + (y/A)^N = s^N, \tag{3}$$

where the power N determines the blockiness of the particle and A determines the aspect ratio. Aspect ratios of up to 12:1 and blockiness factors of up to 20 can be used with our code when performing simulations in 2D. For an early use of super-quadric DEM particles see [25]. In 3D, the particles are modelled here as spheres.

In attempting to model industrial applications we seek to represent accurately as much of the real particle size distribution (PSD) as is feasible. For many applications, particularly in mineral processing, there are significant proportions of the particles with sizes above 10 mm. This makes modelling significant proportions of the PSD possible at present. However, in all cases the smaller sizes of the PSD are neglected. The importance of this approximation depends on both the application, the cutoff size and the proportion of fines omitted. For ball mills, it has been shown [7] that cutoff sizes of 10 mm and below produce negligible changes in either the flow pattern or the power draw of the mill. There is at this time however, no general rule as to what the effects will be for a new application. With the ongoing increase in computer speed and the advent of high-performance parallel computation, the size of the cutoffs in the PSDs required to render simulations feasible will continue to rapidly decline, allowing progressively more accurate modelling of more applications.

The three key parts of the DEM algorithm are:

- A search grid is occasionally used to construct a particle near-neighbour interaction list. Using only particle pairs in the near neighbour list reduces the force calculation to an $O(n)$ operation, where n is the total number of particles. Using such methods allows very large problems to be solved. Depending on the size distribution problems with up to 250,000 particles are now easily solved on single processor workstations.
- The collisional forces for each collision are estimated using the spring-dashpot model for each pair of particles in the near-neighbour list.
- All the collisional and other forces acting on the particles are summed and the resulting equations of motion are integrated for the translational motion:

$$\dot{\mathbf{x}}_i = \mathbf{u}_i, \tag{4}$$

$$\dot{\mathbf{u}}_i = \sum_j \mathbf{F}_{ij} + \mathbf{g}. \tag{5}$$

Similarly the torques produced by the collisions are summed and equations of motion are integrated for the orientation and spin of the particles in 2D:

$$\dot{\theta}_i = \omega_i, \tag{6}$$

$$\dot{\omega}_i = \sum_j M_{ij}, \tag{7}$$

and for just the particle spin in 3D:

$$\dot{\omega}_i = \sum_j \mathbf{M}_{ij}, \tag{8}$$

where $\mathbf{x}_i, \mathbf{u}_i$ and $\mathbf{F}_{ij}$ are the position, velocity and collisional forces on particle i, and ω_i is the vector denoting the particle spin produced by the moments $\mathbf{M}_{ij}$ in 3D and by the scalar moments M_{ij} in 2D and $\mathbf{g}$ is the gravity vector.

Integration of the above set of differential equations is performed using a second-order predictor–corrector scheme. Between 10 and 25 timesteps are required to integrate accurately each collision. This necessitates small timesteps (typically 10^{-4}–10^{-6} s depending on the controlling length and time scales of each problem). If the integration is accurate then the coefficient of restitution from which the damping coefficient was chosen should be recovered.

Quantitative predictions of wear rates and distributions, collision forces, dynamic loads on boundaries, power consumption, torques and flow rates, sampling statistics, mixing and segregation rates and many other quantities can be made from the information available in DEM simulations. For more details on the simulation method and on the data analysis see [5].

3. Shape effects in 2D hopper flow

The hopper used for this study is just over 1.5 m in height, has an internal width of 740 mm, a converging section with a 60° hopper half angle, and an opening for discharge with an internal width of 140 mm. This configuration is shown in Fig. 1 (for the case with super-quadric particles having $N = 6$ and $A = 1.0$).

The particles used have diameters uniformly distributed between 5 and 25 mm. The diameter of the non-circular particles is defined as the largest dimension across the particle. The coefficient of restitution used was 0.3 (appropriate for many types of rocks) and the coefficient of friction was 0.75 (appropriate for many materials with angles of internal friction of around 43°).

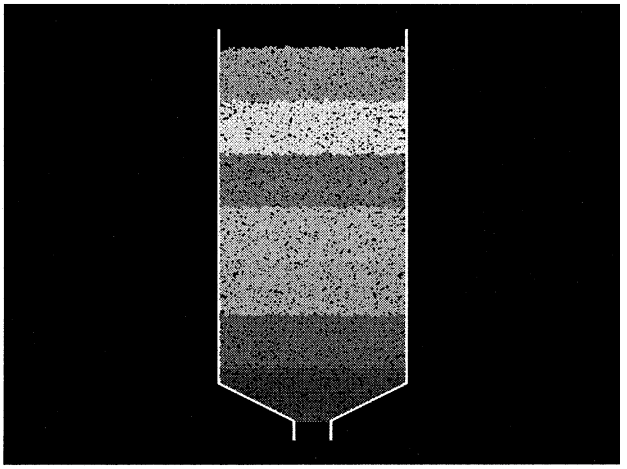

Fig. 1. Configuration for 2D simulations of hopper discharge.

In each case it is necessary to build a microstructure of particles with the specified shapes. For the circular particle case, microstructure is built using one of the fill algorithms available in the custom pre-processor. For other shapes the hopper was filled to a higher level, the particle were scaled to give the appropriate aspect ratios and mapped to give the desired blockiness N and then allowed to settle under gravity. After allowing any oscillations generated by the settling to damp out, the now packed particle microstructure has particles above a height of 1.5 m (measured from the top of the discharge opening) removed and all the residual particle forces, velocities and spins are set to zero. This gives an identical volume of particles for each choice of particle shape in exactly the same starting configuration, which allows careful comparisons of the discharge flows to be made.

For each discharge simulation, the control volume is defined to be periodic in the vertical direction. Particles that have discharged re-enter at the top of the simulation domain and fall onto the top surface of the particles. This means that the mass of material in the hopper is constant in time and gives a constant pressure head driving the flow. This produces a well-defined steady flow that readily allows comparison between cases. If this is not done then there is an approximately linear decline in the discharge mass flow rate and the wall forces have steadily declining amplitude. This would significantly complicate the interpretation of the results.

Several types of data are collected. The particles in the discharge stream are monitored and the time-varying mass flow rate and hopper discharge speed are calculated. The time series of the total force applied by the particles to the hopper structure (in both vertical and horizontal directions) is calculated.

Three series of simulations were performed:

1. Keeping the aspect ratio constant at $A = 1$, the blockiness was varied between 2 (circular) and 12 (essentially square).
2. Keeping the blockiness at $N = 2$ the aspect ratio was varied from 1 down to 0.2. All these particles are elliptical.
3. Keeping the blockiness at $N = 10$ the aspect ratio was varied from 1 down to 0.2. All these particles are essentially rectangular.

The variation of the bulk density of the particles with shape variation is of interest. Normalising the bulk densities by that of the circular particle case, reveals that any non-circularity leads to higher bulk densities. The best packing occurs for $N = 4$. The packing slowly becomes looser with both increasing and decreasing N. For the elliptical particles, the best packing occurs for an aspect ratio of $A = 0.6$. The packing deteriorates quickly with lower aspect ratios, with the $A = 0.2$ case having a relative bulk density of only 0.95. This indicates that the highly elongated particles with random orientations are able to trap 5% more voids than can circular particles. For rectangular particles, the best packing occurs for square ($A = 1$) particles with declining bulk density thereafter. For very elongated particles ($A = 0.2$) the bulk density is around 7% lower than for circular particles.

3.1. Comparison of flow for circular particles with highly non-circular particles

Fig. 2 shows the start of the discharge flow, with very elongated ellipses ($A = 0.2$) on the left and the traditional circular particles on the right. The relative rate of discharge can be judged by

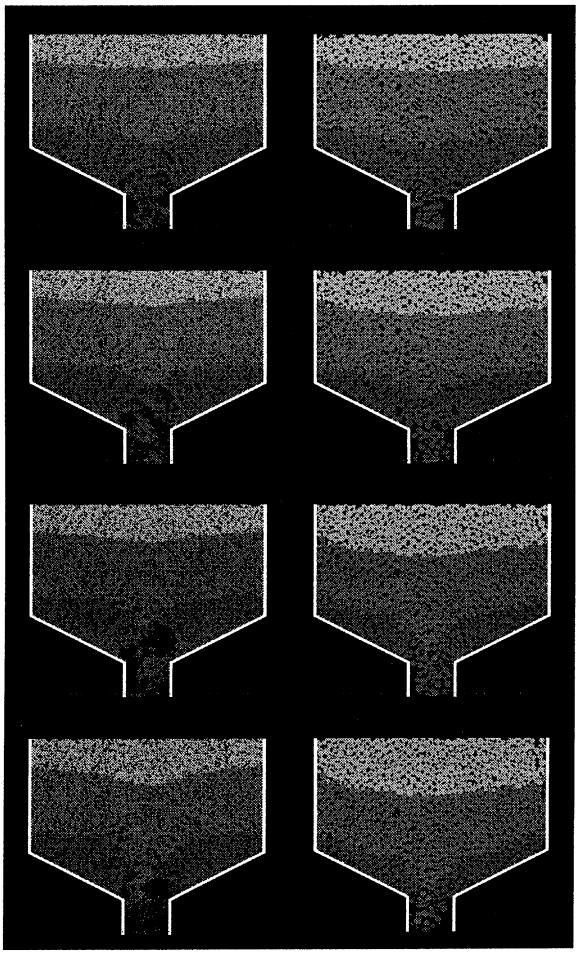

Fig. 2. Flow of elongated elliptical particles with $A = 0.2$ and $N = 2$ (left) and circular particles (right). The top row is at $t = 0.2$ s with each subsequent row spaced by 0.1 s.

the movement of the interfaces between shaded strata. Even at $t = 0.2$ s, the deformation of the lowest interface for the elliptical particles remains highly localised directly above the exit port. In contrast, the circular particle interface is deformed across the width of the hopper forming a reasonably straight-sided V. By $t = 0.5$ s (the last frames of Fig. 2) the deformation of the interface for the elliptical particles barely exceeds the width of the opening below and the majority of the interface is undisturbed. Again in contrast, the circular particle case shows significant flow far to the sides of the exit. The interface maintains its V shape, which deepens in the centre. The circular particles in the computational model flow far too freely, giving a flow that is much closer to that of mass flow even for this very flat bottomed hopper, which would normally be expected to produce a highly concentrated funnel flow. This is unrealistic for real granular materials.

In addition to predicting far more localised central flow (in accordance with observation), the elliptical particles also demonstrate significant strength in resisting shear and nicely illustrate that arching stresses are being reproduced. This can be seen by close inspection of the mode of

microstructure failure above the discharge port. The model shows (at $t = 0.2$ s) the formation of an arch-like void structure directly over the exit as the lower material falls away, but the well-supported material above does not follow immediately. The highly elliptical particle shape gives the microstructure significantly more strength and greatly slows the rate of yielding and flow. In the second set of frames, the microstructure has failed higher up and another chunk of material has begun to descend. Again, this produces significant void structure above and these are arch like in shape, reflecting the well-known arching stresses that support real granular materials in such situations. In the next frame, the material that had previously failed has moved downwards, but a large quasi-stable arch on the right continues to support the granular material on that side. Significant rents in the fabric of the microstructure can be seen to the left and well above the opening. These particles do not flow like discrete particles, but move much more like a fracturing continuum. In contrast, the circular particle flow is always smooth, with each particle moving independently, has negligible changes in the void structure, and barely inhibits the flow of material near the sides. The elliptical particle model thus appears to be capturing a significantly larger proportion of the hopper flow dynamics.

3.2. Effect of blockiness N

Fig. 3 shows the effect of increasing particle blockiness (for constant aspect ratio $A = 1$) on the flow pattern in the lower half of the hopper after 2.5 s. The deformation of the strata illustrates clearly the changes that occur. For circular particles ($N = 2$) the flow is very free and all particles are easily able to exit, with only those within a couple of particle diameters of the wall impeded in any way. This can be seen clearly by the sharp upturn in the interface between the lightest grey particles (at the top) and the dark grey ones (directly below) immediately adjacent to the walls. The lightest grey particles have moved down a significant distance into the hopper. This is very close to mass flow. For $N = 3$, the pattern is broadly similar, but the lightest grey material has not moved so far down into the hopper and the second lightest grey material (the third strata in this figure) no longer reaches the opening by 2.5 s. For $N = 4$ and all higher values, the behaviour is similar, with the lightest grey material travelling progressively less far down into the hopper with increasing N. The shapes of the lower interfaces are broadly unchanged, still being V like with reasonably straight sides. Each of these interfaces also moves slightly higher with each increase in N. The increasing blockiness has a distinct effect by reducing the discharge rate, but perhaps surprisingly does little to change the pattern of the flow, just its rate. This is quite the opposite of the findings for the filling of dragline buckets [6] where the blockiness was shown to have a significant effect in increasing resistance to bucket penetration.

3.3. Effect of aspect ratio A

Comparing the effect of varying aspect ratio for circular particles (left column of Fig. 4) we find that the main effect of increasing A is to slowly increase the levels of the interfaces between shaded strata, but more importantly, to change the shape of these interfaces. For all the previous cases the lower interfaces were V shaped with straight edges. For $A = 0.6$ there is a hint of upward curvature in the interfaces. For $A = 0.4$ this curvature is very clearly defined and indicates that the

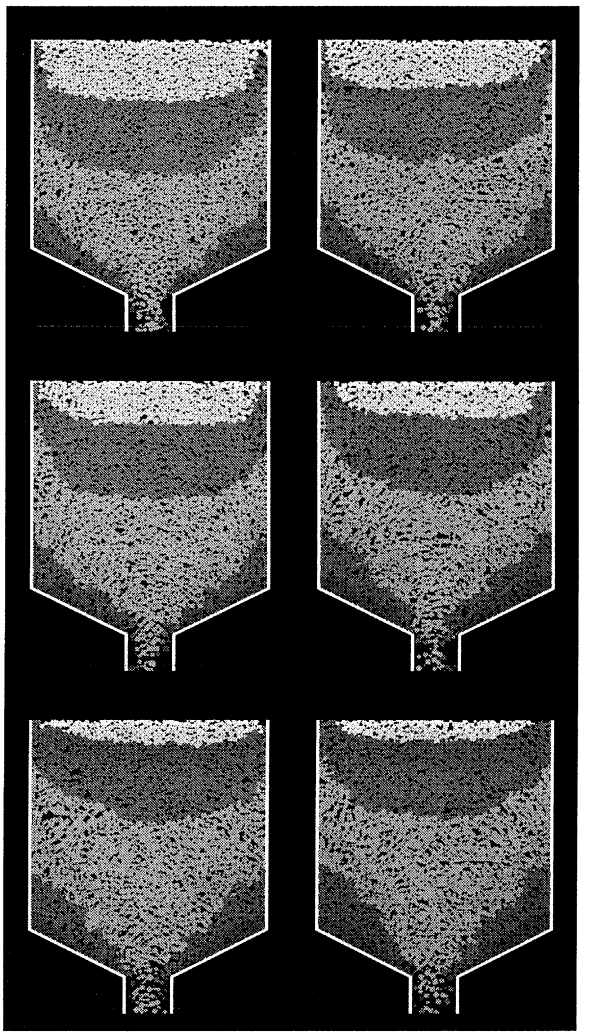

Fig. 3. Discharge pattern at $t = 2.5$ s for increasing blockiness of the particles (from top left to bottom right) $N = 2$, $N = 3$, $N = 4$, $N = 6$, $N = 8$ and $N = 10$.

material strength in the side regions is now becoming strong enough to resist shear and reduce local particle flows. Increasing aspect ratio also appears to reduce the discharge rate slowly.

Examining the effect of increasing aspect ratio A for rectangular particles (right column of Fig. 4) the same qualitative phenomena are observed, but stronger. The flow rates are already much reduced by the blockiness of the particles for $N = 10$ and $A = 1$. Increasing aspect ratio progressively reduces the flow rate further, again shown by the reduced penetration of the lightest grey material into the hopper. More importantly, the lower V-shaped interfaces again start to become curved upwards by $A = 0.6$. In contrast to the elliptical case, the interfaces now become jagged as the yielding consists of discrete failures rather than continuous deformation. For the very elongated squarish case ($A = 0.2$) the change in the interface structure is quite marked. They

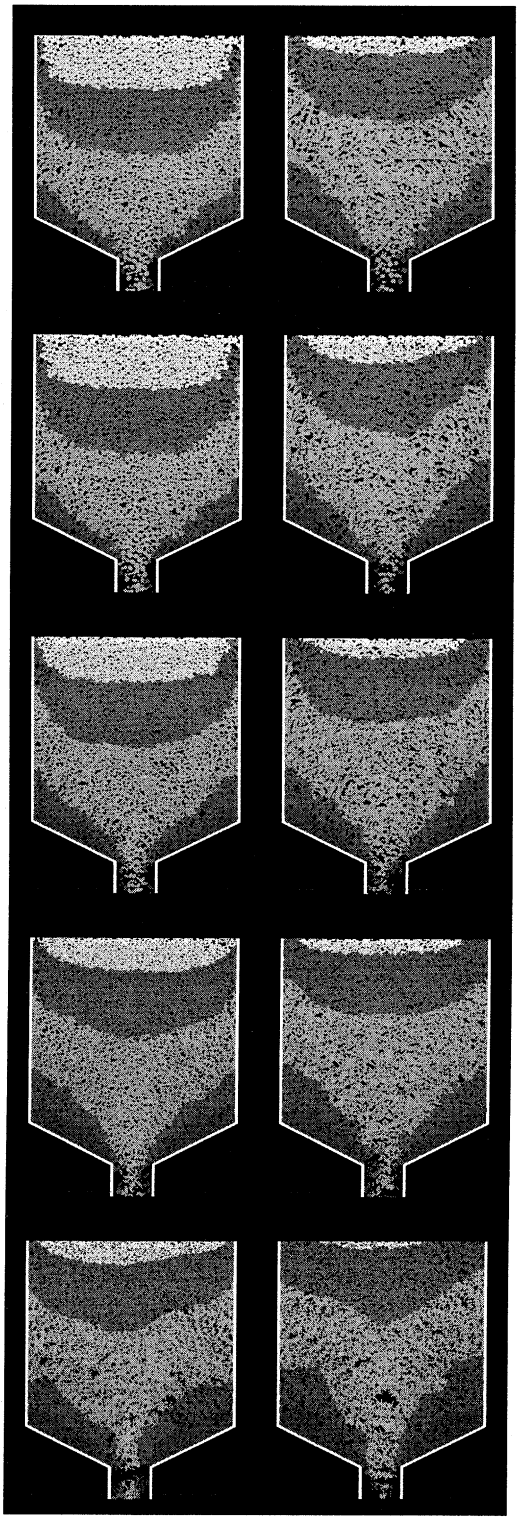

Fig. 4. Discharge pattern for varying particle aspect ratio corresponding to rows (from top to bottom) $A = 1$, $A = 0.8$, $A = 0.6$, $A = 0.4$ and $A = 0.2$. Circular particle cases on the left and rectangular ($N = 10$) particles on the right.

are essentially bi-linear now with a steep central section and very flat side regions. This indicates that there is barely any cumulative movement in this side material. The microstructure strength is now significant. The flow is now becoming concentrated in the central core and is approaching the flow behaviour known as rat-holing, where a narrow funnel in the centre of the hopper empties and new material flows along the top surface and down the rat-hole while all the side material remains stationary. This is an undesirable state, but it is critical that DEM models be able to predict its occurrence. Finally, significant void regions are clearly observable in this last flow-resistant case.

3.4. Variation of hopper discharge rate with particle shape

Fig. 5 shows the average mass flow rate predicted for discharge from the hopper for particles with several values of blockiness. The circular particles produce the highest flow rate since they are the most free flowing. Departures from circularity produce a linear (with N) decline in the mass flow rate, until $N = 8$ after which the subtle variations in particle shape fail to make any further difference to the nature of the flow.

Fig. 6 shows the mass flow rate as a function of the aspect ratio A for elliptic particles (top) and rectangular particles (lower frame). In both cases there is a linear decrease in the mass flow rate with increasing elongation of the particles. For $A = 0.2$ the reduction is around 30%. There is no sign of reduced sensitivity of the mass flow rate occurring for very high aspect ratios.

3.5. Effect of particle shape on the hopper wall forces

Fig. 7 (top) shows the time series of the total force exerted by the circular particles on the hopper. The mean value of this time series is the weight of the particles, which is around 20 kN/m. Even for circular particles there are large fluctuations which average around 50% of the mean.

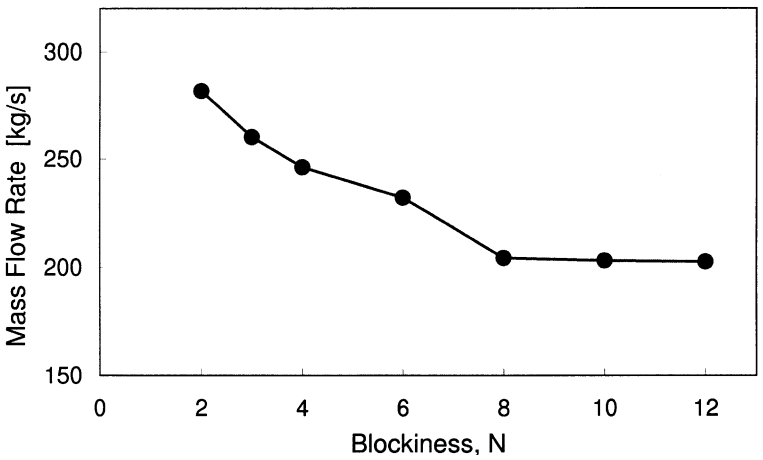

Fig. 5. Mass flow rate from the hopper as a function of particle blockiness.

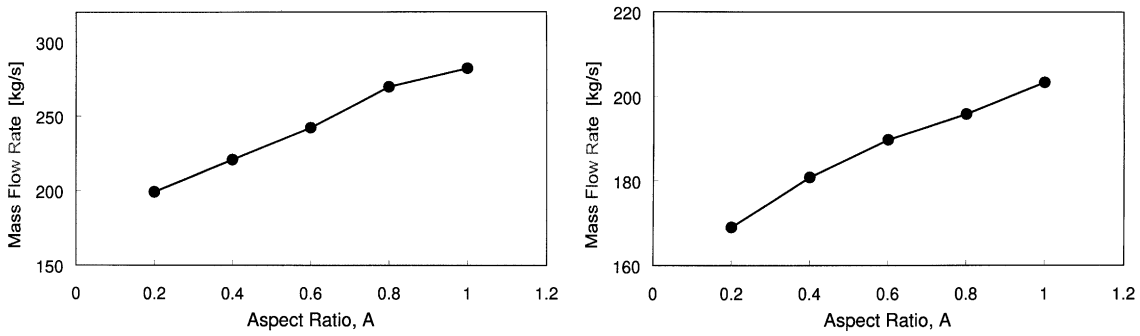

Fig. 6. Variation of mass flow rate with aspect ratio for elliptical (top) and rectangular (bottom) particles.

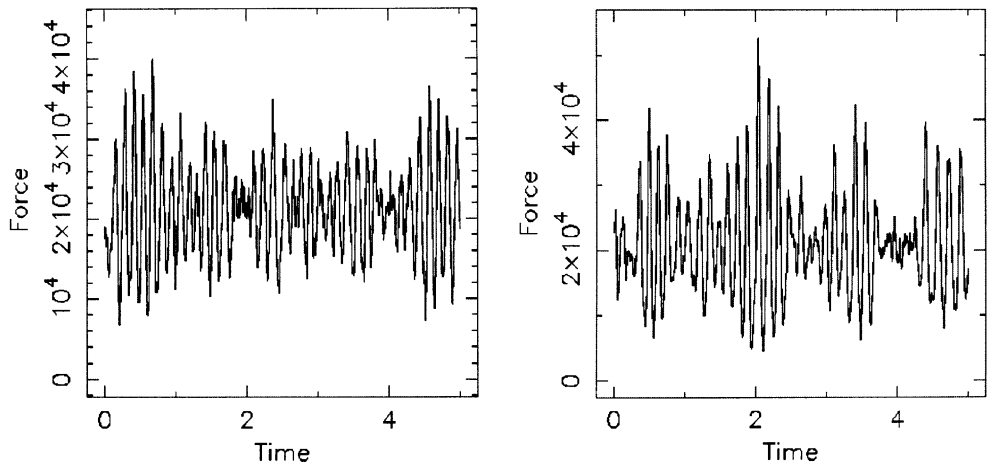

Fig. 7. Vertical force (in N) applied to the walls of the hopper by circular particles (left), and rectangular particles ($N = 10$ and $A = 0.4$) (right) as a function of time (in s).

There is a well-defined periodicity to these fluctuations with a frequency of approximately 7.8 Hz. This is clearly modulated by at least one much longer period oscillation. Close inspection of animations of these flows reveals the source of these fluctuations. The pressure from particles above pushes the particles adjacent to the wall both outwards and down. These particles are supported by friction with the walls and some contacts with particles below. As the hopper discharges and the particle microstructure below re-arranges itself, this lower support steadily diminishes. Eventually, the frictional forces on the walls exceed the Coulomb limits and all the unsupported particles fall abruptly until they come to rest on the particles below. This is known as a slip-stick phenomena and is responsible for silo quaking and honking. It can be clearly seen in the visualisations where large amounts of the upper material remains stationary for some time and then abruptly moves lower. The ability of DEM to predict this phenomena at least qualitatively is encouraging.

Fig. 7 (right) shows the corresponding vertical wall force for elongated blocky material ($N = 10$ and $A = 0.4$). The time series is surprisingly similar with a clearly dominant frequency at around

7.6 Hz. The modulation of the primary frequency is somewhat different and the amplitude of the oscillations is slightly larger.

4. 3D industrial DEM simulations

In this section we describe our approach to modelling geometrically complex industrial flows, including geometry specification, visualisation and parallelisation. Four case studies are presented.

4.1. Pre-processing and visualisation in 3D

Industrial particle flows typically involve particles interacting with boundaries with significant geometric complexity. We have chosen to implement in our simulation procedure a strategy utilising as much commercial pre-processing software as possible. The geometry is initially constructed using a CAD package (e.g. AutoCAD). This geometry is then imported into a commercial mesh generator (e.g. FEMAP or Patran) to construct a standard triangular finite-element surface mesh that then describes the object for the DEM code. (A tetrahedral mesh describing the geometry volume may also be required for visualisation purposes.) Particle-object contact detection then reduces to efficient particle triangular primitive contact detection.

Visualisation of such particulate flows is extremely difficult because of the requirement to render the surfaces of all the particles. Even relatively simple cases, such as the ball mill shown below with around 30,000 particles, require around 3 million polygons to be computed for each time frame. Of these polygons, very few are seen since all but the front particles are obscured. Most commercial CFD visualisation software is unable to distinguish between the particles needed to be drawn and those which are not. Such 3D simulations can take almost as long to visualise as they do to compute. Thus, while parallel DEM simulations involving millions of particles are computationally feasible, they still provide an immense challenge for visualisation.

4.2. Ball mill modelling in three dimensions

Ball mills are large rotating drums (up to around 7 m in diameter) used for grinding rock in the mineral processing and quarrying industries. The rock generally comes from a crusher or perhaps a semi-autogenous (SAG) mill (depending on the design of the milling circuit) and is fed into one end of the mill. Grinding media consisting of steel balls with sizes in the range 50–150 mm are present in the mill along with rock that is still too large to exit through the extraction grate at the opposite end. Particles migrate slowly along the length of the mill, while circulating rapidly with the mill shell in the plane orthogonal to the mill axis. The radial and azimuthal particle motion is assisted by lifter bars attached to the mill shell. Replaceable liner plates are bolted to the shell between the lifters to reduce wear in this hostile environment.

A typical 5 m diameter ball mill consumes around 3–4 MW of power and has an energy efficiency of around only 1–5%. Significant economic and environmental benefits can be obtained by improving this efficiency even slightly. There are also significant costs involved in replacing the liners (commonly made from expensive, wear-resistant, cast molybdenum stainless steel) arising

both from the liner cost and from lost production. Further significant benefits can be obtained through higher downstream recovery if the exit PSDs can be made closer to the optimum for the subsequent flotation processes.

Here we consider the motion of the steel balls in a 3 m axial section of the same 5 m ball mill that has been used in previous 2D simulations [4,7]. There are 23 lifter bars attached around the circumference of the mill and running the full length of the mill. The mill geometry is effectively 2D, but extruded along its axis of rotation. The mill rotates clockwise at some fraction R of the critical rotation rate of 19.5 rpm (based on the 4.8 m internal diameter of the liner), at which an average size ball begins to centrifuge. The charge of 30,000 particles is comprised of 5% (by number) of 200 mm, 47.5% of 100 mm and 47.5% of 75 mm diameter spherical balls, and corresponds to a solid loading of 50%. Periodic boundaries are assumed at the axial ends of the simulation domain, so that the model represents an infinitely long mill.

Fig. 8 shows the positions of the balls (shaded by their velocity) in a mill rotating at $R = 80\%$. Qualitatively, the flow pattern is quite similar to that observed for the 2D cases [4,7]. The toe is on the right and the charge shoulder is elevated on the left. Particles near the mill shell rotate almost rigidly with the mill rotation, until they reach the shoulder. The particles between the lifters are hurled into space and form a well-defined cataracting layer high in the mill. These particles impact heavily on the charge in the toe region and against the liner above. The bulk of the particles avalanche down the steeply inclined slope of the charge. Between the avalanching layer in the middle and the rigidly rotating layer on the outside is a stationary region. The very high shear produced between these layers leads to particle size reduction of rocks in the ball mill by abrasive rubbing, chipping off of sharp corners of the rocks, and by small particles being pinched between the balls.

4.3. The Hicom nutating mill

The grinding process in a Hicom 120 mill is achieved through a unique combination of the grinding chamber geometry and a high-speed nutating motion. Centrifugal accelerations of up to

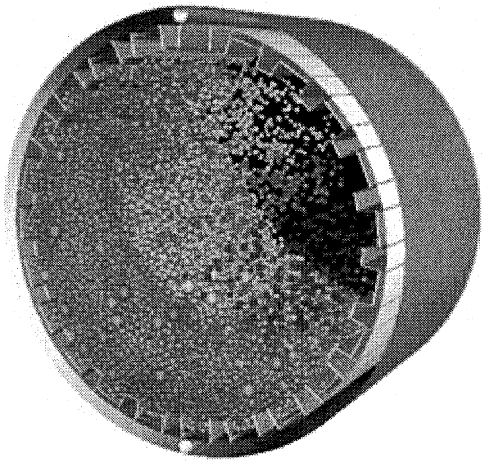

Fig. 8. Instantaneous locations of the balls (shaded by velocity) in a ball mill.

50G and power densities up to 2500 kW/m^3 can be generated, resulting in very high particle breakage rates. Hicom mills can be used for a variety of combination tasks [8,9], and are particularly well suited to energy-efficient, fine grinding down to 10 μm and below.

Insights into the complex motion of the mill charge have been obtained through DEM simulations. In the present study, the grinding chamber is inclined at an angle of 4.75° from vertical, and moves with a nutating motion at a frequency of 730 rpm. In performing this motion, the nutation point at the top of the chamber remains stationary, while points on the chamber below describe circles of diameter increasing with distance from the nutation point. The grinding chamber, which is roughly conical in shape with a hemispherical base, is filled at the top through a 120 mm diameter port. Ground material is discharged through four equally-spaced ports in the side of the chamber. For the present simulations, the 60-l chamber was half-filled with 22,600 spherical particles of size uniformly distributed between 6 and 20 mm diameter.

Fig. 9 shows two snapshots of the mill with a cutaway view from the side. The particles (shaded by velocity) are forced against the interior side wall of the mill by the centrifugal force and are somewhat slumped towards the bottom in response to the comparatively weak gravitational force. As the chamber rotates, the particle charge moves around the inside of the mill. This generates the high shear between particles that results in the grinding process. The motion of the particles is more gentle in the upper section of the mill, since the centrifugal force is comparatively low. In the lower section, the chamber is wider and its displacement from the vertical (caused by the inclination) is larger, leading to much higher particle accelerations and much higher speed impacts. The impact of the particles at the leading edge of the charge with the raised internal ribs is particularly strong. As the charge mass moves over a section of chamber wall containing a discharge port, a pulse of particles is emitted.

Fig. 10 shows the cutaway view from the top of the mill chamber. The rib pattern of the mill liner is clearly observed, as is the shape of the charge. This shape remains relatively invariant, merely rotating with the mill rotation. At the specific time chosen for this figure, a group

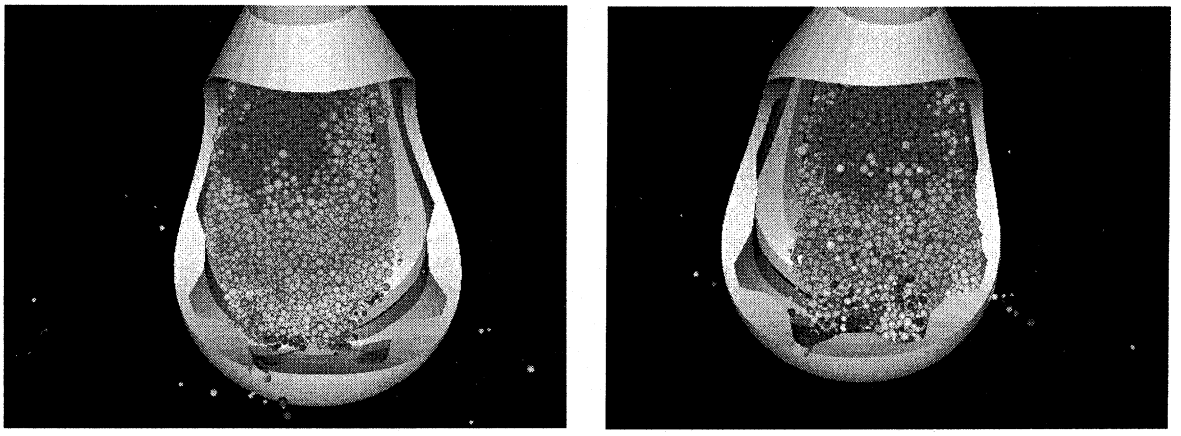

Fig. 9. Side cutaway view, at two different times, of the particles (shaded by velocity) in the Hicom nutating mill.

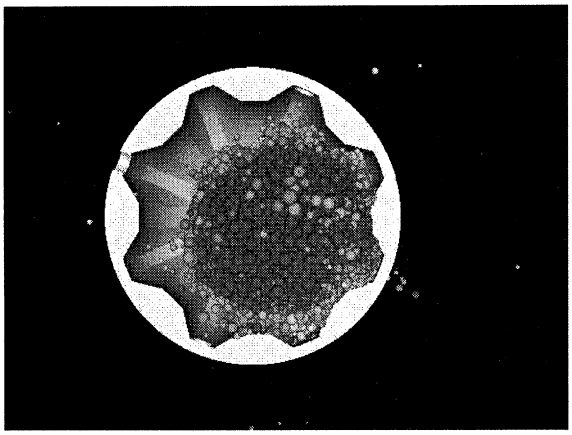

Fig. 10. Top cutaway view of the particles (shaded by velocity) in the Hicom nutating mill.

of particles can be seen just outside the mill having just exited from the lower right discharge port.

4.4. Size separation by a vibrating screen

Vibrating screens are commonly used to separate particles according to their size. Separation is a critical step in most mineral processing operations and the efficiency of this separation has direct implications for both mineral recovery levels and costs.

Particle segregation by one level of a screen is presented here. We consider an 800 mm square section of a screen, 10 mm thick, containing a 12×12 array of 40 mm square holes. The screen is covered by a mixture of 8000 spherical particles, with sizes uniformly distributed between 10 and 60 mm, to a depth of 400 mm. Periodic boundaries have been applied at each of the sides of the screen to simulate a screen having a much larger area. The screen is oscillated upwards and to one side with a frequency of 3 Hz, a vertical amplitude of 50 mm, and a sideways amplitude of 20 mm. The oscillations in the two directions are in phase so that the screen moves sinusoidally in a straight line inclined at 22° to the vertical.

Fig. 11 shows the screen at two times during the vibration cycle. As it moves upwards, smaller particles move freely through the holes in the screen. The flow of small particles continues throughout the screen's upward movement, although the rate declines slightly. As the screen moves down, the particles lag behind and loose contact with the screen. The flow of small particles through the screen abates until the screen reaches its lowest point and the particles crash back into the screen producing a surge of smaller particles through the screen. This behaviour leads to a regular pulsing flow of fines from the screen. Also observed in Fig. 11 is the well-defined size segregation of the material on top of the screen, with the larger (dark grey) particles being dominant near the upper surface. The progressive percolation of small particles from the upper regions to the region adjacent to the screen ensures a continual supply of fines to flow through the screen. The ability of DEM to simulate this type of flow demonstrates the method's potential for use as a design tool for such industrial particle handling equipment.

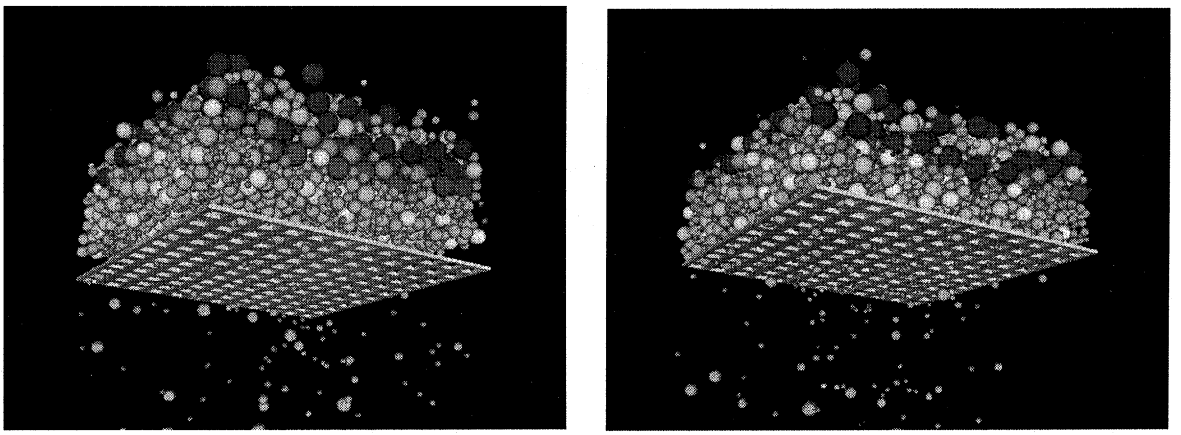

Fig. 11. Particle locations (shaded by size) at two different times during the vibration cycle of the screen.

4.5. Discharge from a cylindrical hopper

Hoppers are often used for particle storage in the mineral processing and manufacturing industries. They consist of large storage areas with some type of discharge region below. A particularly common type is a cylindrical hopper with a single central discharge port. DEM simulations have been undertaken for a cylindrical hopper, 3 m high and 1.5 m in diameter, having a discharge port of 400 mm diameter. The hopper chute angle of the conical section is 45°. The particles are uniformly distributed in size between 40 and 80 mm diameter, with 25,000 required to fill the hopper.

Fig. 12 shows the location of the particles (shaded by initial vertical position) at one time during the discharge. In this view the particles and the hopper have been cut away to show details of the particle distribution within the centre of the hopper. Even at this early time during the discharge, the preferential flow down the centre of the hopper is clearly discernible.

Many materials will not flow in hoppers with such shallow hopper chute angles. In order to avoid excessively tall structures, it is quite common to have multiple discharge ports from multiple conical sections with a much steeper chute angle. Multiple discharge ports can also be used if large ranges of flow rates are required or if the material needs to flow to different destinations.

DEM simulations have been performed for a cylindrical four-port hopper, 4 m high and 1.5 m in diameter. The four discharge ports each have a diameter of 250 mm and a conical chute angle of 60°. The particles are uniformly distributed in size between 25 and 60 mm. For this case, 70,000 particles are required to fill the hopper, and particles discharge through all four ports.

Fig. 13 shows two representative views at different times during the simulation. Again, the particles are shaded by their initial vertical position. The view on the left of Fig. 13 shows the hopper as translucent to enable the behaviour of the particles adjacent to the hopper shell to be studied. On the right of Fig. 13 is shown a cutaway view that allows the behaviour of the closest particles to be more easily identified.

DEM modelling can be used to assess the effect of using only some of the discharge ports and to assess the impact of various combinations of these on the forces applied by the flowing granular

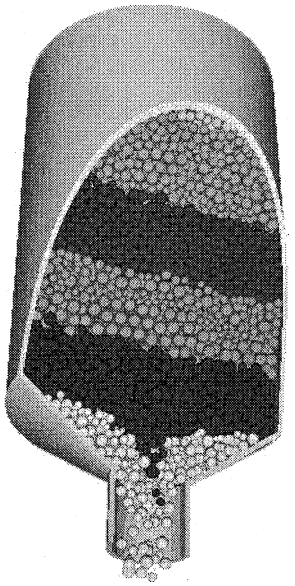

Fig. 12. Cutaway view of the discharging of particles (shaded in layers) from a cylindrical single-port hopper.

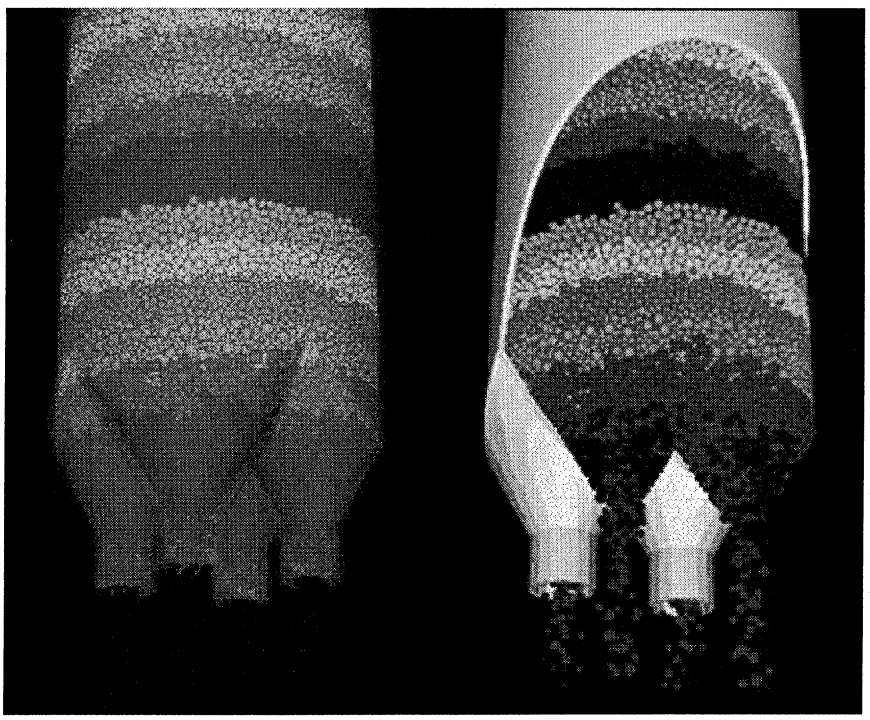

Fig. 13. Two views, at different times, of discharging of particles (shaded in layers) from a cylindrical four-port hopper.

material to the hopper structure. The existence of stagnant regions can also be identified along with other impediments to flow, which are much more common in multiple discharge hoppers.

5. Parallelisation

Since the earlier DEM simulations involved relatively modest numbers of particles (<100,000), the computations were easily performed in a reasonable time on a single-processor workstation. As the geometric and physical complexity of the modelling increases, so does the computational resources required. The simulation of, for example, one million non-spherical particles in a complex 3D geometry, including the effects of breakage and/or cohesion, is thus not reasonably performed by a single processor. However, the required level of computational power can, in principle, be obtained through the application of parallel computing to the DEM simulations.

As a preliminary study of the development of a parallel DEM code, the parallelisation of 2D simulations has been investigated. The underlying parallel algorithm is based on domain decomposition. The simulation domain is divided into subdomains by a simple slicing parallel to either the x or y axis. Choosing the number of subdomains equal to the number of processors available, data associated with particles in the same subdomain are stored in the same processor's memory. The computational effort depends on the number of collisions between particles, which is closely related to the number of particles. Assuming processors of equal performance, to achieve load balance (in order to minimise synchronisation delays) the subdomains are chosen to contain the same number of particles.

Of the different parallel programming models available, message passing (using either the MPI or PVM library) has been chosen for the present implementation. This model provides both low communication overhead (leading to higher parallel performance) and a high level of code portability (since message passing is available on essentially all parallel computer systems). Communication between processors associated with interactions of particles across the subdomain boundaries is optimised by copying a layer of 'ghost' particles from the neighbouring subdomains, as shown in Fig. 14.

Using the above-described parallel algorithm, after the input data is read and distributed to the appropriate processor memory, each processor performs essentially the same grid search and collision calculation as for the sequential algorithm. Periodic communication between processors is necessary to update the ghost particle information. It is important to note that the subdomain boundaries are not fixed in physical space, but are automatically moved to satisfy the load balancing requirements. Such dynamic load balancing is essential for an efficient parallel DEM implementation.

The performance of this parallel implementation has been assessed on the Swiss-T1 machine, consisting of a cluster of 64 Digital Alpha 21264 processors connected via a high-bandwidth, low-latency network [12]. Fig. 15 (top) shows, in a log–log plot, the measured wall-clock time required to simulate 0.1 s (about 1100 time steps) of the flow of 200,000 particles in a 2D hopper. It can be observed that the time required to perform the necessary computational work decreases linearly with the number of processors employed. The communication required to transfer data between processors, however, is seen to be approximately independent of the number of processors employed. Nevertheless, since the communication time is always significantly less than the

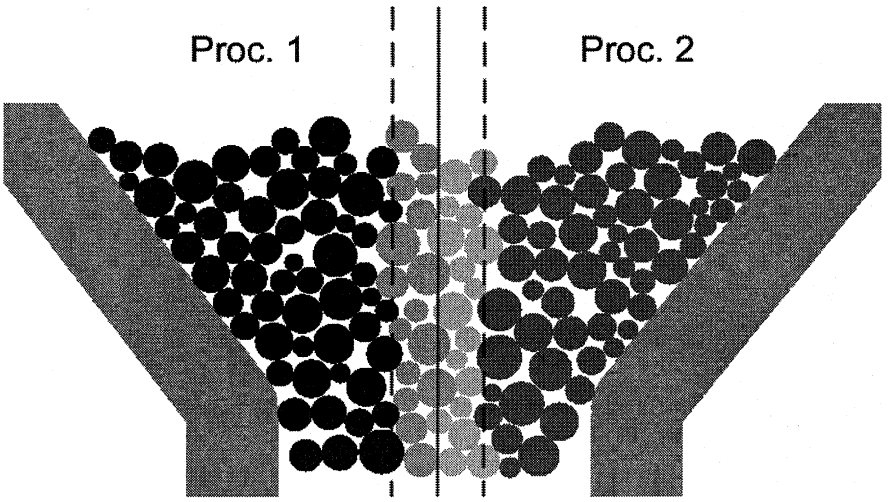

Fig. 14. Particles shaded according to storage location in memory for a two-processor decomposition. Light shades denote ghost particles.

computation time (for up to the 48 processors used), the total time required to perform the simulation decreases essentially linearly with the number of processors. This leads to an approximately linear performance speedup, as shown in Fig. 15 (bottom). Finally, it can be observed from Fig. 15 (top) that the time required to perform the grid search is only a very small fraction of the total simulation time over the entire range of number of processors considered in this study.

It should be noted that large 3D flow simulations will involve significantly more particles than has been considered in the present relatively modest size 2D problem. Since the ratio of communication to computation time decreases with the number of particles, it is anticipated that such large 3D simulations will yield close to linear scaling for even greater numbers of processors of a parallel computer system with characteristics similar to those of the Swiss-T1 machine.

6. Conclusion

Hopper discharge has been modelled using DEM in 2D for a wide selection of particle shapes in order to understand the effect that shape has on these flows. Circular particles are a particularly special case that do not well represent real granular materials. Circular particles have little resistance to shear or frictional forces. These forces cause the particle microstructure to yield prematurely via a rolling mode of failure. This causes the flow rates to be over-estimated and always leads to excessively fluid-like mass flow in the hoppers.

The effect of both particle aspect ratio and blockiness have been investigated independently and then together. The blockiness of the material surprisingly makes little difference to the actual pattern of the particle flow. Increasing blockiness does increase the resistance to flow and reduces the flow rate by around 28%, but the flow pattern is still closer to mass flow than to real funnel flow. The reduction in flow rate plateaus for $N > 8$; the hopper flows are not sensitive to any

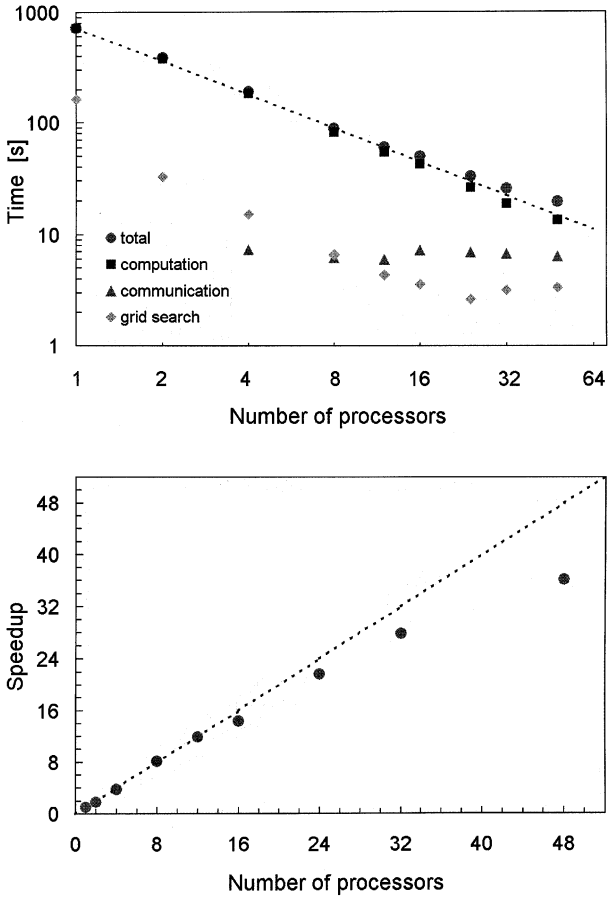

Fig. 15. Computational time required for the individual tasks of a 2D DEM simulation (top), and performance speedup (bottom) as a function of the number of processors employed. The dashed lines represents linear scaling.

further subtle increases in the angularity of the particles. This is quite different to the behaviour found for dragline bucket filling. Increasing the aspect ratio of the particles has a stronger effect on the flow. The behavioural changes are similar for elliptical particles and for rectangular particles. Changing from circular particles to elliptical ones with a 5:1 aspect ratio ($A = 0.2$) leads not only to a 29% reduction in the flow rate, but also to substantial changes in the structure of the particle flow. These particles no longer behave as free-flowing independent particles but behave more like deforming, fracturing continua. Yielding leads to tearing of the microstructure fabric, producing substantial voids that are quasi-stable and supported by arching stresses. A number of these cases also lead to spontaneous stable bridging. These particles essentially generate funnel flow.

The present study has thus demonstrated that particle shape appears to be extremely important in hopper flows. This extension of DEM to use non-circular particles represents one amongst many important steps that are required before DEM can confidently predict all the phenomena that occur in hoppers. Other effects still to be understood include the locking of 3D

microstructures, the effect of particle asymmetry, the effect of cohesion, the effects of differing wall-particle to particle-particle friction properties and the effect of micro-roughness on the walls of the hopper.

The 3D modelling capabilities of our DEM code have also been described. Difficulties that arise from generating the geometries and visualising the resulting particulate systems, and the methodology used to parallelise the DEM code, have been discussed. The 3D examples presented indicate that DEM modelling is now sufficiently advanced that it can make useful contributions to process optimisation and equipment design. Simulations of the charge flow in a 5 m ball mill and a nutating mill demonstrate that complicated geometries executing complex motion can be modelled easily. Simulations of flow through a vibrating screen and discharge from single- and four-port cylindrical hoppers illustrate the potential of DEM to handle diverse aspects of particle handling equipment.

Acknowledgements

The study of the Hicom nutating mill were performed under contract with CH Warman Techlink. Part of the parallelisation study was undertaken while one of the authors (MLS) was a Visiting Scientist at the Ecole Polytechnique Fédérale de Lausanne; access to the Swiss-T1 computer system during this study is gratefully acknowledged.

References

[1] G.C. Barker, Computer simulations of granular materials, in: A. Mehta (Ed.), Granular Matter: An Inter-Disciplinary Approach, Springer, Berlin, 1994.
[2] C.S. Campbell, Rapid granular flows, Ann. Rev. Fluid Mech. 22 (1990) 57–92.
[3] P.W. Cleary, The filling of dragline buckets, Math. Eng. Ind. 7 (1998) 1–24.
[4] P.W. Cleary, Predicting charge motion, power draw, segregation, wear and particle breakage in ball mills using discrete element methods, Miner. Eng. 11 (1998) 1061–1080.
[5] P.W. Cleary, Discrete element modelling of industrial granular flow applications, TASK Quart. – Scientific Bull. 2 (1998) 385–416.
[6] P.W. Cleary, DEM simulation of industrial particle flows: case studies of dragline excavators, mixing in tumblers and centrifugal mills, Powder Technol. 109 (2000) 83–104.
[7] P.W. Cleary, Charge behaviour and power consumption in ball mills: sensitivity to mill operating conditions, linear geometry and charge composition, Int. J. Miner. Process. 63 (2001) 79–114.
[8] D.I. Hoyer, J.M. Boyes, High-intensity fine and ultrafine grinding in the Hicom mill, in: Proc. XV CMMI Congress, Johannesburg, SAIMM, vol. 2, 1994, pp. 435–441.
[9] D.I. Hoyer, R.E. Morgan, High-intensity size reduction in the Hicom mill, in: Proc. Chemeca 96, Sydney, 1996.
[10] J.M. Holst, J.M. Rotter, J.Y. Ooi, G.H. Rong, Numerical modelling of silo filling. II: discrete element analysis, J. Eng. Mech. 125 (1999) 104–110.
[11] Y. Kaneko, T. Shiojima, M. Horio, Numerical analysis of particle mixing characteristics in a single helical ribbon agitator using DEM simulation, Powder Technol. 108 (2000) 55–64.
[12] P. Kuonen, R. Gruber, Parallel computer architectures for commodity computing and the Swiss-Tx machine, EPFL Supercomput. Rev. 11 (1999) 3–11.
[13] P.A. Langston, U. Tuzun, D.M. Heyes, Discrete element simulation of internal stress and flow fields in funnel flow hoppers, Powder Technol. 85 (1995) 153–169.

[14] B.K. Mishra, R.K. Rajamani, The discrete element method for the simulation of ball mills, App. Math. Model 16 (1992) 598–604.
[15] B.K. Mishra, R.K. Rajamani, Simulation of charge motion in ball mills. Part 1: experimental verifications, Int. J. Mineral Process. 40 (1994) 171–186.
[16] B.K. Mishra, Some applications of discrete element method in mineral engineering, Met. Mater. Process. 10 (1998) 369–378.
[17] M. Moakher, T. Shinbrot, F.J. Muzzio, Experimentally validated computations of flow, mixing and segregation of non-cohesive grains in 3D tumbling blenders, Powder Technol. 109 (2000) 58–71.
[18] A.V. Potapov, C.S. Campbell, Computer simulation of hopper flow, Phys. Fluids 8 (1996) 2884–2894.
[19] P. Radziszewsky, S. Morrell, Fundamental discrete element charge motion model validation, Miner. Eng. 11 (1998) 1161–1178.
[20] G.H. Ristow, Outflow rate and wall stress for two-dimensional hoppers, Physica A 235 (1997) 319–326.
[21] G.H. Rong, S.C. Negi, J.C. Jofriet, Simulation of flow behaviour in bulk solids in bins. Part 2: shear bands, flow corrective inserts and velocity profiles, J. Agric. Eng. Res. 62 (1995) 257–269.
[22] J. Schäfer, S. Dippel, D.E. Wolf, Force schemes in simulation of granular material, J. Phys. I France 6 (1996) 5–20.
[23] M.A. Van Nierop, G. Glover, A.L. Hinde, M.H. Moys, A discrete element method investigation of the charge motion and power draw of an experimental two-dimensional mill, Int. J. Miner. Process. 61 (2001) 77–92.
[24] O.R. Walton, Numerical simulation of inelastic frictional particle–particle interaction, in: M.C. Roco (Ed.), Particulate Two-Phase Flow, Butterworth-Heineman, London, 1994, pp. 884–911, Chpt. 25.
[25] J.R. Williams, A. Pentland, Super-quadrics and modal dynamics for discrete elements in interactive design, Int. J. Comp. Aided Eng. Software Eng. Comp. 9 (1992) 115–127.
[26] C. Wightman, M. Moakher, F.J. Muzzio, O.R. Walton, Simulation of flow and mixing of particles in a rotating and rocking cylinder, AIChE J. 44 (1998) 1266–1276.